Ultrafast carbon monoxide photolysis and heme spin-crossover in myoglobin via nonadiabatic quantum dynamics

Falahati et al.

State	Label	ANO-RCC-VDZ	Mixed basis set	Absolute Difference
1	^{5}MC	0.70	0.82	0.12
2	^{5}MC	0.74	0.86	0.12
3	^{3}MC	0.89	0.92	0.02
4	^{5}MC	1.40	1.41	0.01
5	^{3}MC	1.43	1.43	0.00
6	^{3}MC	1.51	1.44	0.06
7	^{3}MC	1.62	1.69	0.06
8	^{3}MC	1.86	1.84	0.01
9	^{3}MC	1.90	1.89	0.01
10	^{1}MC	1.90	2.00	0.10
11	^{3}ML	2.15	2.34	0.19
12	^{1}MC	2.35	2.43	0.09
13	^{1}MC	2.36	2.45	0.08
14	$^3Q_1$	2.43	2.46	0.03
15	^{5}ML	2.48	2.66	0.18
16	$^3Q_2$	2.49	2.47	0.02
17	^{3}ML	2.56	2.57	0.01
18	^1Q_x	2.73	2.71	0.02
19	^1Q_y	2.79	2.71	0.07
20	^{1}ML	2.83	2.93	0.10

Supplementary Table 1. Basis set effect. Basis set size effect of the absorption spectrum of Hb-CO using ANO-RCC-VDZ basis set and a mixed basis set consisting of a ANO-RCC-VTZP for Iron with 6s5p3d contractions, ANO-RCC-VDZP for nitrogens and the carbon monoxide and a ANO-RCC-VDZ for the rest of the atoms.

State	Label	Full virtual CASPT2	Frozen virtual CASPT2	Absolute Difference
1	^{5}MC	0.70	0.42	0.28
2	^{5}MC	0.74	0.46	0.28
3	^{3}MC	0.89	0.79	0.10
4	^{5}MC	1.40	1.00	0.40
5	^{3}MC	1.43	1.23	0.20
6	^{3}MC	1.51	1.25	0.27
7	^{3}MC	1.62	1.58	0.04
8	^{3}MC	1.86	1.65	0.21
9	^{3}MC	1.90	1.72	0.18
10	^{1}MC	1.90	1.99	-0.09
11	^{3}ML	2.15	1.77	0.38
12	^{1}MC	2.35	2.35	0.00
13	^{1}MC	2.36	2.38	-0.02
14	$^3Q_1$	2.43	1.96	0.47
15	^{5}ML	2.48	2.19	0.29
16	$^3Q_2$	2.49	2.32	0.17
17	^{3}ML	2.56	2.43	0.13
18	^1Q_x	2.73	2.79	0.06
19	^1Q_y	2.79	2.85	-0.06
20	^{1}ML	2.83	2.64	0.19

Supplementary Table 2. Benchmark of CASPT2. Comparison of CASPT2 using the full virtual space and CASPT2 freezing 116 virtual orbitals. In both cases, 37 core orbitals are frozen. The computational cost of CASPT2 calculations in the full space of orbitals is too demanding for practical uses. Therefore, we reduced the space of configurations in the perturbative treatment by freezing the core orbitals and 116 highest virtual orbitals.

State	Energy (eV)	Osc. Strength	Interpretation	Label	Symmetry
1	0.70	0.000	$(d_{yz},d_{xy}) \rightarrow (d_{x^2-y^2},d_{z^2})$	^{5}MC	E
2	0.74	0.000	$(d_{xz},d_{xy}) \rightarrow (d_{x^2-y^2},d_{z^2})$	^{5}MC	E
3	0.89	0.000	$d_{xy} \rightarrow d_{x^2-y^2}$	^{3}MC	B_2
4	1.40	0.000	$(d_{xz},d_{yz}) \rightarrow (d_{x^2-y^2},d_{z^2})$	^{5}MC	
5	1.43	0.000	$d_{xz} \rightarrow d_{z^2}$	^{3}MC	E
6	1.51	0.000	$d_{yz} \rightarrow d_{z^2}$	^{3}MC	E
7	1.62	0.000	$d_{xy} \rightarrow d_{z^2}$	^{3}MC	A_2
8	1.86	0.000	$d_{yz} \rightarrow d_{x^2-y^2}$	^{3}MC	E
9	1.90	0.000	$d_{xz} \rightarrow d_{x^2-y^2}$	^{3}MC	E
10	1.90	0.000	$d_{xy} \rightarrow d_{x^2-y^2}$	^{1}MC	B_2
11	2.15	0.000	$(a_2,d_{yz},d_{xy}) \rightarrow (e,d_{x^2-y^2},d_{z^2})$	^{3}ML	
12	2.35	0.000	$d_{yz} \rightarrow d_{z^2}$	^{1}MC	E
13	2.36	0.000	$d_{xy} \rightarrow d_{z^2}$	^{1}MC	E
14	2.43	0.000	$a_2 \rightarrow e$	$^3Q_1$	E
15	2.48	0.000	$(a_2,d_{yz},d_{xy}) \rightarrow (e,d_{x^2-y^2},d_{z^2})$	^{5}ML	
16	2.49	0.000	$a_2 \rightarrow e$	$^3Q_2$	E
17	2.56	0.000	$(a_1,d_{yz},d_{xy}) \rightarrow (e,d_{x^2-y^2},d_{z^2})$	^{3}ML	
18	2.73	0.015	$a_2 \rightarrow e$ / $a_1 \rightarrow e$	^1Q_x	E
19	2.79	0.010	$a_2 \rightarrow e$ / $a_1 \rightarrow e$	^1Q_y	E
20	2.83	0.000	$(a_2,d_{yz}) \rightarrow (e,d_{z^2})$	^{1}ML	

Supplementary Table 3. Heme–CO Absorption spectrum. Absorption spectrum of Heme–CO model calculated at the CASSCF(10,9)/MS-CASPT2/ANO-RCC-VDZ level. The transitions in the interpretation are represented according to orbital excitations from the ground state closed-shell configuration of the leading MS-CASPT2 configuration. The labels used are either metal-centred (MC), metal-ligand-transition (ML) and Q for the porphyrin states. The symmetry assignments are only approximate, considering that the distal hystidin has only a spectator role and the states can be assigned according to a C_{4v} point group.

State	Energy (eV)	Interpretation	Label
1	0.65	$(a_1,d_{xz},d_{yz})\rightarrow(d_{z^2},e,d_{x^2-y^2})$	^{3}ML
2	0.67	$(a_1,d_{xz},d_{yz})\rightarrow(d_{z^2},e,d_{x^2-y^2})$	^{5}ML
3	0.72	$(a_1,d_{xz},d_{xy})\rightarrow(d_{z^2},e,d_{x^2-y^2})$	^{5}ML
4	0.72	$(a_1,d_{yz},d_{xy})\rightarrow(d_{z^2},e,d_{x^2-y^2})$	^{3}ML
5	0.72	$(a_1,d_{yz},d_{xy})\rightarrow(d_{z^2},e,d_{x^2-y^2})$	^{5}ML
6	0.74	$(a_1,d_{yz},d_{xy})\rightarrow(d_{z^2},e,d_{x^2-y^2})$	^{3}ML
7	0.76	$(d_{xz},d_{xy})\rightarrow(d_{z^2},d_{x^2-y^2})$	^{3}MC
8	0.82	$(a_1,d_{xz},d_{xy})\rightarrow(d_{z^2},e,d_{x^2-y^2})$	^{5}ML
9	0.83	$(a_1,d_{xz},d_{yz})\rightarrow(d_{z^2},e,d_{x^2-y^2})$	^{5}ML
10	0.84	$(a_1,d_{xy},d_{yz})\rightarrow(d_{z^2},e,d_{x^2-y^2})$	^{5}ML
11	0.85	$(a_1,d_{xz},d_{xy})\rightarrow(d_{z^2},e,d_{x^2-y^2})$	^{3}ML
12	0.90	$(d_{yz},d_{xy})\rightarrow(d_{z^2},d_{x^2-y^2})$	^{3}MC
13	0.91	$(a_1,d_{xy},d_{yz})\rightarrow(d_{z^2},e,d_{x^2-y^2})$	^{5}ML
14	0.94	$(a_2,d_{xy},d_{yz},d_{xz})\rightarrow(d_{z^2},d_{z^2},e,d_{x^2-y^2})$	^{3}ML
15	0.94	$(a_2,d_{yz})\rightarrow(d_{z^2},e)$	^{1}ML
16	0.96	$(a_1,d_{xy},d_{xz})\rightarrow(d_{z^2},e,d_{x^2-y^2})$	^{5}ML
17	0.99	$(a_1,d_{xy},d_{xz})\rightarrow(d_{z^2},e,d_{x^2-y^2})$	^{5}ML
18	1.00	$(a_2,d_{xy},d_{yz},d_{xz})\rightarrow(d_{z^2},d_{z^2},e,d_{x^2-y^2})$	^{3}ML
19	1.02	$(d_{xy},d_{xz})\rightarrow(d_{z^2},d_{x^2-y^2})$	^{3}MC
20	1.07	$(d_{xz},d_{yz})\rightarrow(d_{z^2},d_{x^2-y^2})$	^{3}MC
21	1.10	$(d_{xz},d_{yz})\rightarrow(d_{z^2},d_{x^2-y^2})$	^{3}MC
22	1.15	$(d_{xy},d_{yz})\rightarrow(d_{z^2},d_{x^2-y^2})$	^{3}MC
23	1.17	$(a_2,d_{yz})\rightarrow(d_{z^2},e)$	^{1}ML
24	1.18	$(d_{yz},d_{xz})\rightarrow(d_{z^2},d)$	^{1}MC

Supplementary Table 4. Reduced model absorption spectrum. Absorption spectrum of porphyrin-Fe-CO model (without the imidazole ring) calculated at the CASSCF(10,9)/MS-CASPT2/ANO-RCC-VDZ level. The transitions in the interpretation are represented according to orbital excitations from the ground state closed-shell configuration of the leading MS-CASPT2 configuration. The labels used are either metal-centred (MC), metal-ligand-transition (ML) and Q for the porphyrine states. The symmetry assignments are only approximate, considering that the distal hystidine has only a spectator role and the states can be assigned according to a C_{4v} point group.

State	Energy (eV)	Interpretation	Label
1	-1.76	$(d_{xz},d_{xy})\rightarrow(d_{z^2},d_{x^2-y^2})$	^{5}MC
2	-1.73	$(d_{xz},d_{yz})\rightarrow(d_{z^2},d_{x^2-y^2})$	^{5}MC
3	-1.09	$(d_{xy},d_{yz})\rightarrow(d_{z^2},d_{x^2-y^2})$	^{5}MC
4	-0.66	$d_{xz} \rightarrow d_{z^2}$	^{3}MC
5	-0.57	$d_{yz} \rightarrow d_{z^2}$	^{3}MC
6	-0.18	$d_{xy} \rightarrow d_{z^2}$	^{3}MC
7	-0.01	$(d_{xz},d_{yz})\rightarrow(d_{x^2-y^2}, d_{x^2-y^2})$	^{3}MC
8	0.17	$(a_2,d_{yz},d_{xz})\rightarrow(d_{z^2},e,d_{x^2-y^2})$	^{3}ML
9	0.18	$(a_2,d_{yz},d_{xz})\rightarrow(d_{z^2},e,d_{x^2-y^2})$	^{3}ML
10	0.20	$(a_2,d_{yz},d_{xy})\rightarrow(d_{z^2},e,d_{x^2-y^2})$	^{3}ML
11	0.20	$(a_2,d_{yz},d_{xy})\rightarrow(d_{z^2},e,d_{x^2-y^2})$	^{3}ML
12	0.20	$(d_{xy},d_{yz},d_{xz})\rightarrow(d_{z^2},d_{z^2},d_{x^2-y^2})$	^{5}MC
13	0.28	$(d_{xy},d_{yz},d_{xz})\rightarrow(d_{z^2},d_{x^2-y^2},d_{x^2-y^2})$	^{5}MC
14	0.29	$(a_2,d_{xy},d_{xz})\rightarrow(d_{z^2},e,d_{x^2-y^2})$	^{5}ML
15	0.32	$(a_1,d_{yz},d_{xy})\rightarrow(d_{z^2},e,d_{x^2-y^2})$	^{3}ML
16	0.33	$(a_2,d_{yz},d_{xz})\rightarrow(d_{z^2},e,d_{x^2-y^2})$	^{5}ML
17	0.35	$(a_2,d_{xy},d_{xz})\rightarrow(d_{z^2},e,d_{x^2-y^2})$	^{3}ML
18	0.35	$(a_2,d_{yz},d_{xz})\rightarrow(d_{z^2},e,d_{x^2-y^2})$	^{5}ML
19	0.36	$(a_2,d_{xy},d_{xz})\rightarrow(d_{z^2},e,d_{x^2-y^2})$	^{5}ML
20	0.36	$(a_2,d_{xy},d_{xz})\rightarrow(d_{z^2},e,d_{x^2-y^2})$	^{3}ML
21	0.46	$(a_2,d_{yz},d_{xy})\rightarrow(d_{z^2},e,d_{x^2-y^2})$	^{5}ML
22	0.48	$d_{yz} \rightarrow d_{z^2}$	^{1}MC
23	0.49	$d_{xy} \rightarrow d_{x^2-y^2}$	^{3}MC
24	0.49	$(a_2,d_{yz},d_{xy})\rightarrow(d_{z^2},e,d_{x^2-y^2})$	^{5}ML
25	0.52	$(a_1,d_{yz},d_{xz})\rightarrow(d_{z^2},e,d_{x^2-y^2})$	^{3}ML
26	0.54	$(a_1,d_{xz},d_{xy})\rightarrow(d_{z^2},e,d_{x^2-y^2})$	^{5}ML
27	0.57	$d_{yz} \rightarrow d_{x^2-y^2}$	^{3}MC
28	0.58	$d_{xz} \rightarrow d_{z^2}$	^{1}MC
29	0.59	$d_{xz} \rightarrow d_{x^2-y^2}$	^{3}MC
30	0.63	$(a_1,d_{xz},d_{yz})\rightarrow(d_{z^2},e,d_{x^2-y^2})$	^{5}ML

Supplementary Table 5. Decarboxy model absorption spectrum. Spectrum of the imidazole-Heme model calculated at the CASSCF(10,9)/MS-CASPT2/ANO-RCC-VDZ level. The ground state is now a quintet state, but the configurations are represented as excitations to the singlet closed shell configuration. The transitions in the interpretation are represented according to orbital excitations from the ground state closed-shell configuration of the leading MS-CASPT2 configuration. The labels used are either metal-centred (MC), metal-ligand-transition (ML) and Q for the porphyrine states.

	Gas phase			QM/MM		
State	Energy (eV)	Osc. Strength	Interpretation	Energy (eV)	Osc. Strength	Interpretation
1	1.602	0.0000	$d_{yz} \rightarrow e_x$	1.067	0.0002	$d_{xy} \rightarrow d_{x^2-y^2}$
2	1.795	0.0000	$d_{xz} \rightarrow e_y$	1.154	0.0011	$d_{xy} \rightarrow e_y$
3	1.825	0.0001	$(d_{xz}, \pi) \rightarrow (e_y, d_{x^2-y^2})$	1.188	0.0012	$d_{xz} \rightarrow e_x$
4	2.547	0.0001	$\pi \rightarrow e_y$	1.257	0.0012	$d_{yz} \rightarrow e_x$
5	2.604	0.0000	$(d_{yz}, \pi) \rightarrow (e_x, d_{x^2-y^2})$	1.353	0.0008	$d_{yz} \rightarrow d_{z^2}$
6	2.805	0.0000	$(d_{xz}, \pi) \rightarrow (e_y, d_{x^2-y^2})$	1.729	0.0001	$d_{xy} \rightarrow d_{z^2}$
7	2.858	0.0000	$(d_{xz}, \pi) \rightarrow (e_x, d_{x^2-y^2})$	2.062	0.0000	$d_{yz} \rightarrow e_y$
8	2.919	0.0001	$(d_{yz}, \pi) \rightarrow (e_x, d_{z^2})$	2.094	0.0001	$d_{yz} \rightarrow e_x$
9	3.036	0.0001	$d_{yz} \rightarrow e_y$	2.137	0.0001	$d_{yz} \rightarrow e_x$
10	3.063	0.0000	$d_{xz} \rightarrow e_x$	2.350	0.0000	$(d_{xy}, \pi) \rightarrow (e_x, d_{x^2-y^2})$
11	3.074	0.0000	$\pi \rightarrow e_x$	2.423	0.0002	$(d_{xy}, \pi) \rightarrow (e_y, d_{x^2-y^2})$

Supplementary Table 6. Effect of the protein on the absorption spectrum. Comparison of the singlet manifold absorption spectrum of full Heme–CO calculated in the gas phase and at the QM/MM level employing the CASSCF(10,9)/MS-CASPT2/ANO-RCC-VDZ method. The transitions in the interpretation are represented according to orbital excitations from the ground state closed-shell configuration of the leading MS-CASPT2 configuration.

State	CT	MC	LC	MLCT	LMCT
1	8.4	91.5	0.1	7.7	0.7
2	13.1	86.5	0.4	9.7	3.4
3	12.8	86.8	0.4	9.6	3.2
4	80.5	3.7	15.9	9.3	71.2
5	0.8	0.0	99.2	0.1	0.8
6	0.8	0.0	99.2	0.1	0.7
7	72.2	18.9	9.0	71.1	1.1
8	52.7	34.8	12.5	51.3	1.4
9	84.9	2.0	13.1	2.4	82.6
10	85.6	3.3	11.0	6.5	79.1
11	12.7	87.0	0.3	11.6	1.1
12	18.9	79.4	1.7	13.8	5.1
13	13.2	86.3	0.5	11.7	1.4
14	11.7	88.0	0.3	8.1	3.6
15	11.7	88.0	0.3	8.3	3.4
16	11.9	87.6	0.5	8.5	3.4
17	20.7	74.6	4.7	16.9	3.8
18	91.7	0.4	8.0	0.2	91.4
19	38.4	61.1	0.4	36.2	2.2
20	55.1	44.4	0.5	53.5	1.6
21	87.8	3.9	8.3	19.4	68.4
22	76.2	2.3	21.5	11.6	64.6
23	86.7	5.1	8.3	22.0	64.7
24	9.5	90.0	0.5	4.9	4.6
25	37.0	60.7	2.2	32.4	4.6
26	69.3	29.7	1.1	67.8	1.5
27	91.9	0.4	7.7	1.6	90.3
28	83.7	5.6	10.7	10.7	73.0
29	83.0	5.5	11.6	35.9	47.1
30	11.3	88.4	0.3	8.2	3.1
31	11.3	88.4	0.3	8.1	3.3
32	69.2	25.8	5.0	43.1	26.1
33	12.9	86.1	1.0	4.3	8.6
34	11.4	88.5	0.1	10.5	0.9

Supplementary Table 7. State character analysis. Analysis of singlet one-particle transition density matrices between S0 and an excited state. The descriptors shown are the percentage of charge transfer (CT), metal-centered (MC), ligand-centered (LC), metal-to-ligand charge-transfer (MLCT) and ligand-to-metal charge-transfer (LMCT). Here, the ligand is considered as the porphyrin, the imidazole and the carbon monoxide. Calculations have been performed with TheoDore [http://theodore-qc.sourceforge.net].

Dynamics:	1	2	3	4	5	6	7	8	9	10
Mode										
8	0.0000	2.2086	1.5679	1.6863	2.5719	0.9910	1.2120	0.9525	1.5832	0.9146
12	0.0000	-0.4742	-0.4310	-0.8618	-0.1105	-0.4513	0.4665	-0.8952	0.1435	-0.8237
16	0.0000	-0.5391	-0.3823	0.4011	-0.9246	-0.5033	-0.7360	-0.4054	-0.4926	0.1645
17	0.0000	-0.3425	-0.0658	-0.2078	0.2837	0.7531	0.1011	0.3937	0.1641	0.6317
18	0.0000	-0.1482	0.2775	0.1946	0.5238	-0.1025	0.0816	0.4920	0.7240	-0.3165
21	0.0000	-0.7377	-0.5452	0.4596	-0.2184	0.2309	0.4338	-0.4165	-0.4131	-0.6170
22	0.0000	0.1569	-0.3785	0.5238	0.1211	0.3889	-0.6952	0.1619	-0.4442	0.5767
23	0.0000	-1.0742	-1.1350	-0.6131	-0.5799	-0.5441	0.1255	-0.1479	0.1814	-0.6622
26	0.0000	-0.2251	0.5508	0.1869	-0.4410	-0.0811	-0.0355	0.3209	0.0182	-0.0112
27	0.0000	-0.2665	0.0038	-0.6745	0.2467	-0.0803	-0.1198	-0.6621	-0.3058	-0.1000
28	0.0000	0.0648	0.2926	-0.0249	0.4756	0.3370	-0.6968	0.4235	-0.0985	-0.1914
33	0.0000	-1.0949	-1.2167	-0.8405	-0.8761	-1.0008	-0.5934	-0.5653	-0.8813	-1.1415
35	0.0000	0.4457	0.2481	0.2740	0.1896	0.0275	-0.1423	0.0850	-0.0243	-0.0763
36	0.0000	0.1459	0.0943	-0.4371	-0.4038	-0.3701	-0.2683	-0.3734	-0.0788	-0.0327
122	0.0000	0.0046	0.0032	0.0017	0.0068	0.0107	0.0012	0.0009	0.0027	0.0036

Supplementary Table 8. Quantum dynamics initial conditions. Set of 10 initial conditions extracted from the molecular dynamics simulation on *Equus caballus* myoglobin-CO complex.[1] The values correspond to the displacement of the corresponding normal mode. These have been obtained by extracting the cartesian coordinates from different MD snapshots and projecting them in the basis of normal modes used to parametrize the model Hamiltonian.

	τ_{S-T}	τ_{T-Q}	τ_Q
1	60.63	252.77	9.40
2	81.71	428.40	22.15
3	69.13	471.50	19.98
4	80.58	450.39	29.81
5	72.21	473.90	24.34
6	89.61	422.64	28.65
7	55.36	497.29	29.12
8	67.79	430.95	31.87
9	74.13	477.34	32.06
10	111.32	386.60	29.97

Supplementary Table 9. Photodynamic timescales. Time scales (in femtoseconds) for the reactions singlet→triplet (τ_{S-T}), triplet→quintet (τ_{T-Q}) and ^{1}Q→^{1}MLCT (τ_Q) reactions.

	Hb-CO (S=0)		Heme-CO (S=0)		deoxyHb (S=2)	Experimental
Mode	Frequency (cm^{-1})	Assignment	Irrep	Frequency (cm^{-1})	Frequency (cm^{-1})	
1	23.968	Histidine rotation			24.050	
2	45.903	Histidine tortion y			27.573	
3	60.377	Porphyrine OOP	B_2	50.556	61.344	
4	63.552	Porphyrine OOP	B_1	51.072	76.511	
5	71.554	CO torsion x	E	73.124		
6	75.489	CO torsion y	E	73.124		
7	81.311	Histidine torsion x + CO torsion x			39.843	
8	90.431	Porphyrine OOP + Fe OOP	A_1	103.024		
9	159.815	Porphyrine OOP	E	155.859	154.110	
10	161.986	Porphyrine OOP	E	155.859		
11	196.854	Porphyrine + Histidine torsion y			128.362	
12	208.513	Histidine			171.12	
13	213.640	Histidine			164.262	
14	215.485	Porphyrine IP	B_1	224.988	169.725	
15	231.528	Porphyrine IP	B_2	230.836	200.559	
16	263.807	Fe IP + Porphyrine	E	250.744	224.089	
17	264.796	Fe IP + Porphyrine	E	250.744	229.581	
18	286.811	Porphyrine + Fe OOP + CO	A_1	261.785	240.334	
19	303.997	Porphyrine OOP	A_2	297.757	314.693	
20	315.167	Porphyrine OOP	B_2	290.045		
21	318.540	Histidine + Fe + CO	E	294.998	252.307	
22	323.305	Porphyrine IP + Histidine + Fe	E	294.998	529.615	
23	356.220	Porphyrine IP	A_1	355.681	351.828	
24	365.077	Porphyrine IP	E	368.402	390.730	
25	365.623	Porphyrine IP	E	368.402	390.455	
26	376.370	Fe-CO	A_1	371.630	365.044	
27	407.592	Porphyrine IP	E	411.154	390.455	
28	409.115	Porphyrine IP	E	411.154		
29	426.112	Porphyrine IP	B_1	432.304	417.838	
30	428.517	Porphyrine IP	A_2	431.203		
31	452.146	Porphyrine OOP	E	452.146	459.769	
32	454.646	Porphyrine OOP	E	454.646	453.576	
33	488.045	Fe OOP-CO dissociation	A_1	546.790	505	Biophys. J. 80, 2372 (2001)
34	498.135	Porphyrine OOP	B_1	494.800	500.870	
35	574.101	CO y	E	512.680		

Supplementary Table 10. Vibrational modes. Comparison of the vibrational modes of Hb-CO , Heme-CO and deoxyHb models in their lowest energy state. Modes are calculated at the B3LYP/LAND2Z level. The assignment is based on the Hb-CO vibrations, classified as out-of-plane (OOP) in-plane (IP) porphyrine distortions; and histidine or CO contributions if present. The vibrations of the Heme-CO are classified according to the irreducible representations of the C_{4v} point group.

	Hb-CO (S=0)		Heme-CO (S=0)		deoxyHb (S=2) Experimental
Mode	Frequency (cm^{-1})	Assignment	Irrep	Frequency (cm^{-1})	Frequency (cm^{-1})
36	578.414	CO x	E	512.680	
37	627.151	Histidine OOP			628.629
38	663.391	Histidine OOP	E	693.760	666.358
39	690.059	Histidine OOP	E	693.760	683.881
40	690.282	Porphyrine OOP	B_2	689.033	689.358
41	694.239	Histidine - Porphyrine	E	729.814	696.314
42	694.826	Porphyrine OOP	E	729.814	694.491
43	707.539	Porphyrine OOP	A_2	707.080	709.262
44	713.224	Porphyrine OOP	B_1	711.495	712.473
45	727.126	Porphyrine OOP	E	729.814	722.003
46	727.296	Porphyrine OOP	E	729.814	722.951
47	733.864	Porphyrine OOP	A_1	735.822	729.998
48	738.498	Porphyrine IP	A_1	740.495	733.763
49	751.022	Porphyrine IP	B_2	751.596	749.306
50	755.698	Porphyrine IP	E	757.182	754.127
51	757.599	Porphyrine IP	E	757.182	751.727
52	766.822	Histidine			771.125
53	795.577	Porphyrine OOP	A_1	802.791	795.159
54	808.014	Porphyrine OOP	E	815.213	809.935
55	808.947	Porphyrine OOP	E	815.213	806.644
56	820.252	Porphyrine IP	E	820.252	817.218
57	820.475	Porphyrine OOP	B_2	826.982	821.368
58	821.592	Porphyrine IP	E	821.592	817.216
59	822.077	Porphyrine IP	A_2	823.925	816.016
60	839.722	Porphyrine IP	B_1	840.489	
61	864.232	Histidine			861.810
62	894.401	Porphyrine OOP	B_1	904.909	895.379
63	903.468	Porphyrine OOP	E	914.968	902.507
64	903.495	Porphyrine OOP	E	914.968	903.938
65	911.925	Histidine			908.850
66	912.551	Porphyrine OOP	A_1	925.183	913.185
67	940.174	Histidine			936.449
68	945.844	Porphyrine OOP	A_2	951.693	945.263
69	950.152	Porphyrine OOP	E	957.084	949.281
70	950.668	Porphyrine OOP	E	957.084	949.989

Supplementary Table 10 continued.

	Hb-CO (S=0)		Heme-CO (S=0)		deoxyHb (S=2) Experimental
Mode	Frequency (cm^{-1})	Assignment	Irrep	Frequency (cm^{-1})	Frequency (cm^{-1})
71	953.022	Porphyrine OOP	B_1	959.950	952.690
72	960.326	Histidine			955.155
73	1004.994	Porphyrine IP	A_1	1004.670	1010.627
74	1007.752	Porphyrine IP	E	1006.664	997.052
75	1008.293	Porphyrine IP	E	1006.664	997.969
76	1012.775	Porphyrine IP	B_2	1012.925	1016.082
77	1017.522	Porphyrine IP	A_2	1014.043	1011.281
78	1045.157	Porphyrine IP	E	1044.314	1022.711
79	1045.473	Porphyrine IP	E	1044.314	1028.178
80	1066.686	Porphyrine IP	B_1	1063.944	1041.765
81	1079.060	Histidine			1071.447
82	1093.939	Porphyrine IP	E	1098.789	1090.598
83	1095.198	Porphyrine IP	B_2	1099.920	1090.008
84	1095.738	Porphyrine IP	E	1098.789	1092.252
85	1100.602	Porphyrine IP	A_1	1104.292	1097.432
86	1120.780	Histidine			1100.953
87	1153.970	Histidine			1149.020
88	1176.726	Porphyrine IP	A_2	1172.944	1178.186
89	1183.063	Porphyrine IP	E	1182.383	1180.107
90	1184.091	Porphyrine IP	E	1182.383	1177.492
91	1185.583	Histidine			1178.377
92	1210.142	Porphyrine IP	B_2	1208.288	1193.620
93	1226.794	Porphyrine IP	B_1	1232.760	1227.271
94	1281.238	Porphyrine IP	E	1290.151	1272.409
95	1285.932	Porphyrine IP	E	1290.151	1269.135
96	1286.115	Histidine			1282.184
97	1336.933	Porphyrine IP	E	1348.808	1329.042
98	1341.099	Porphyrine IP	E	1348.808	1324.720
99	1358.770	Histidine			1356.220
100	1364.077	Porphyrine IP	A_2	1362.268	1357.120
101	1280.021	Porphyrine IP	B_1	1384.785	1372.126
102	1382.059	Porphyrine IP	A_1	1387.072	1363.478
103	1386.884	Porphyrine IP	A_2	1389.220	1386.338
104	1423.294	Porphyrine IP	E	1414.903	1415.336
105	1426.226	Porphyrine IP	E	1414.903	1419.005
106	1428.835	Porphyrine IP	B_2	1419.971	1417.301
107	1435.426	Histidine			1424.590
108	1479.803	Porphyrine IP	E	1494.741	1466.759
109	1483.509	Porphyrine IP	A_1	1494.379	1459.360
110	1485.770	Porphyrine IP	E	1494.741	1459.156

Supplementary Table 10 continued.

Hb-CO (S=0)			Heme-CO (S=0)		deoxyHb (S=2) Experimental
Mode	Frequency (cm^{-1})	Assignment	Irrep	Frequency (cm^{-1})	Frequency (cm^{-1})
111	1500.737	Histidine			1495.243
112	1521.576	Porphyrine IP	B_1	1535.518	1495.212
113	1534.326	Porphyrine IP	B_2	1534.326	1522.337
114	1566.881	Histidine			1558.140
115	1575.189	Porphyrine IP	E	1586.025	1552.244
116	1578.558	Porphyrine IP	E	1586.025	1557.822
117	1600.825	Porphyrine IP	A_1	1611.892	1579.420
118	1619.396	Porphyrine IP	E	1641.536	1589.724
119	1629.202	Porphyrine IP	E	1641.539	1595.611
120	1642.585	Porphyrine IP	A_2	1656.540	1610.861
121	1684.060	Porphyrine IP	B_2	1707.299	1653.108
122	1978.449	CO	A_1	1971.316	
123	3207.619	Porphyrine		H-wagging	
124	3207.893	Porphyrine		H-wagging	
125	3208.446	Porphyrine		H-wagging	
126	3208.955	Porphyrine		H-wagging	
127	3250.737	Porphyrine		H-wagging	
128	3250.849	Porphyrine		H-wagging	
129	3250.881	Porphyrine		H-wagging	
130	3251.577	Porphyrine		H-wagging	
131	3277.367	Porphyrine		H-wagging	
132	3277.826	Porphyrine		H-wagging	
133	3277.875	Porphyrine		H-wagging	
134	3278.256	Porphyrine		H-wagging	
135	3319.446	Histidine		H-wagging	
136	3347.201	Histidine		H-wagging	
137	3356.502	Histidine		H-wagging	
138	3690.449	Histidine		H-wagging	

Supplementary Table 10 continued.

Mode 1	Mode 2	Mode 3	$V_{i,j,k}$ (cm^{-1})
22	8	8	-14.6863
22	16	16	-11.7859
22	18	18	-80.8503
22	21	21	-77.1663
23	22	8	-22.7241
23	22	21	-15.1951
23	23	22	-68.5081
26	22	8	-38.1493
26	22	18	-10.7142
26	26	22	-115.6509
27	12	8	-13.1565
27	16	16	14.9445
27	21	21	-82.3505
27	23	12	16.8431
27	23	23	13.1509
27	26	12	29.1195
27	27	22	-17.8932
28	26	26	11.9516
33	26	22	-35.7878
33	33	22	11.3630
35	23	22	21.1882
35	27	21	18.4865
35	35	22	16.5150
36	22	12	33.5126
36	27	8	-31.1431
122	122	17	35.9359

Supplementary Table 11. Anharmonic vibrational couplings. Third-order anharmonic mode couplings $V_{i,j,k}$ in cm^{-1} in the space of normal modes used to expand our vibronic model Hamiltonian. Only couplings with absolute value larger than 10 cm^{-1} are shown.

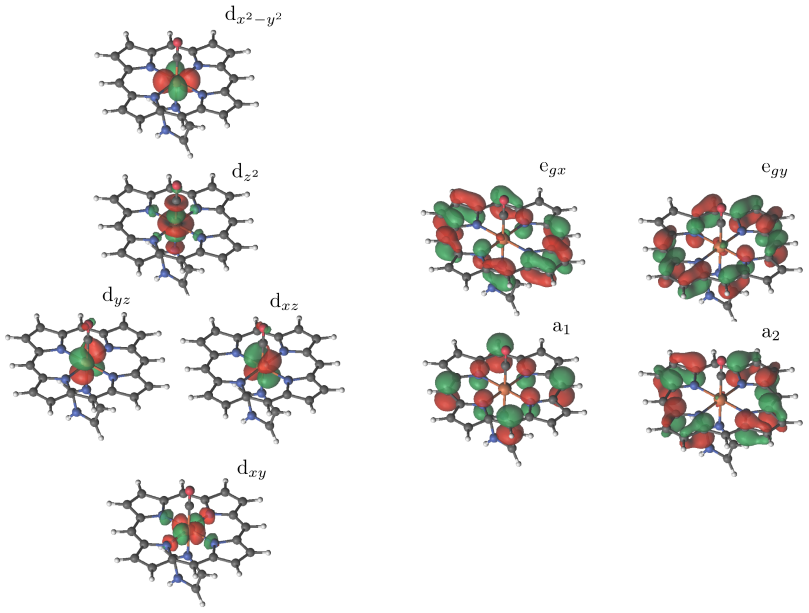

Supplementary Figure 1. Active space orbitals. Active space orbitals employed in the CASSCF(10,9)/CASPT2 calculations. Two occupied orbitals and two virtual orbitals correspond to the porphyrin moiety and two occupied and two virtuals for the Fe centre.

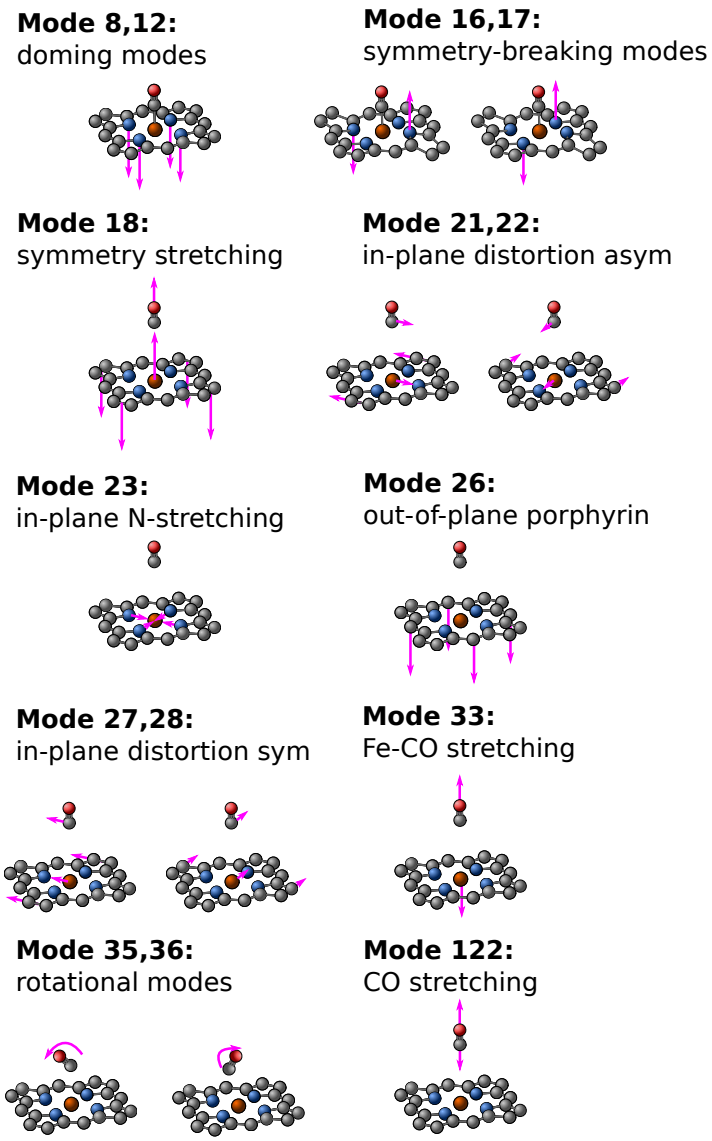

Supplementary Figure 2. Normal modes in the vibronic model. Schematic representation of the 15 vibrational modes included in the vibronic model with their interpretation. For a detailed analysis of all normal modes, see Supplementary Table 10.

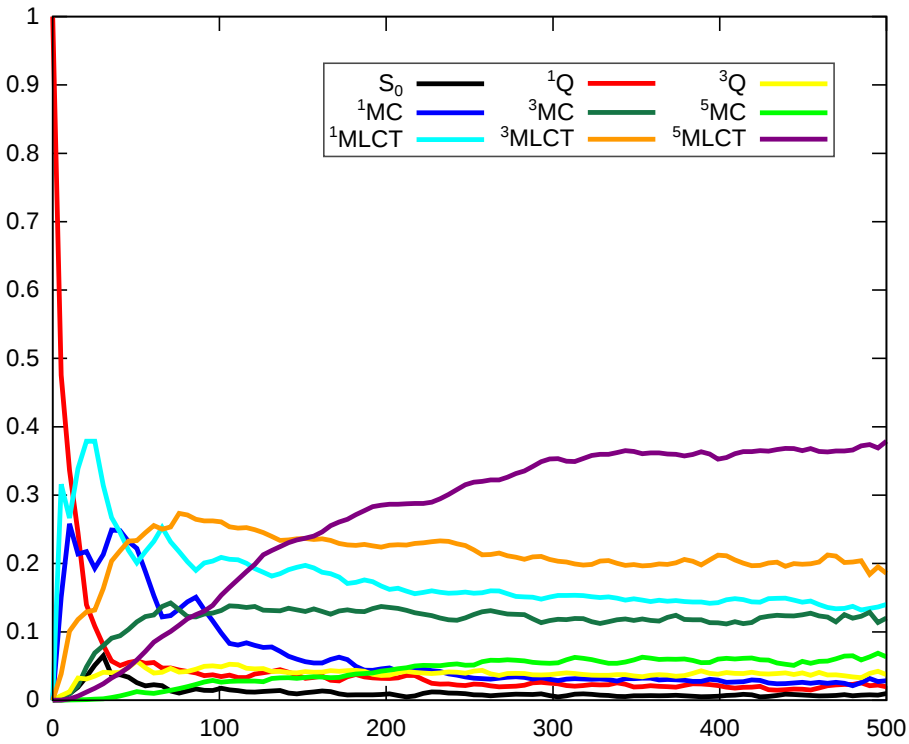

Supplementary Figure 3. Detailed full model population evolution. Evolution of diabatic populations in detail. The population evolution contains the ground state (S0), the singlet metal centred (dark blue), the singlet metal-ligand charge transfer band (light blue), the singlet Q state (red), the triplet metal centred (dark green), the triplet metal-ligand charge transfer (orange), the triplet Q state (yellow), the quintet metal centred state (light green) and the metal-ligand charge transfer (purple). Time (x-axis) is in femtoseconds.

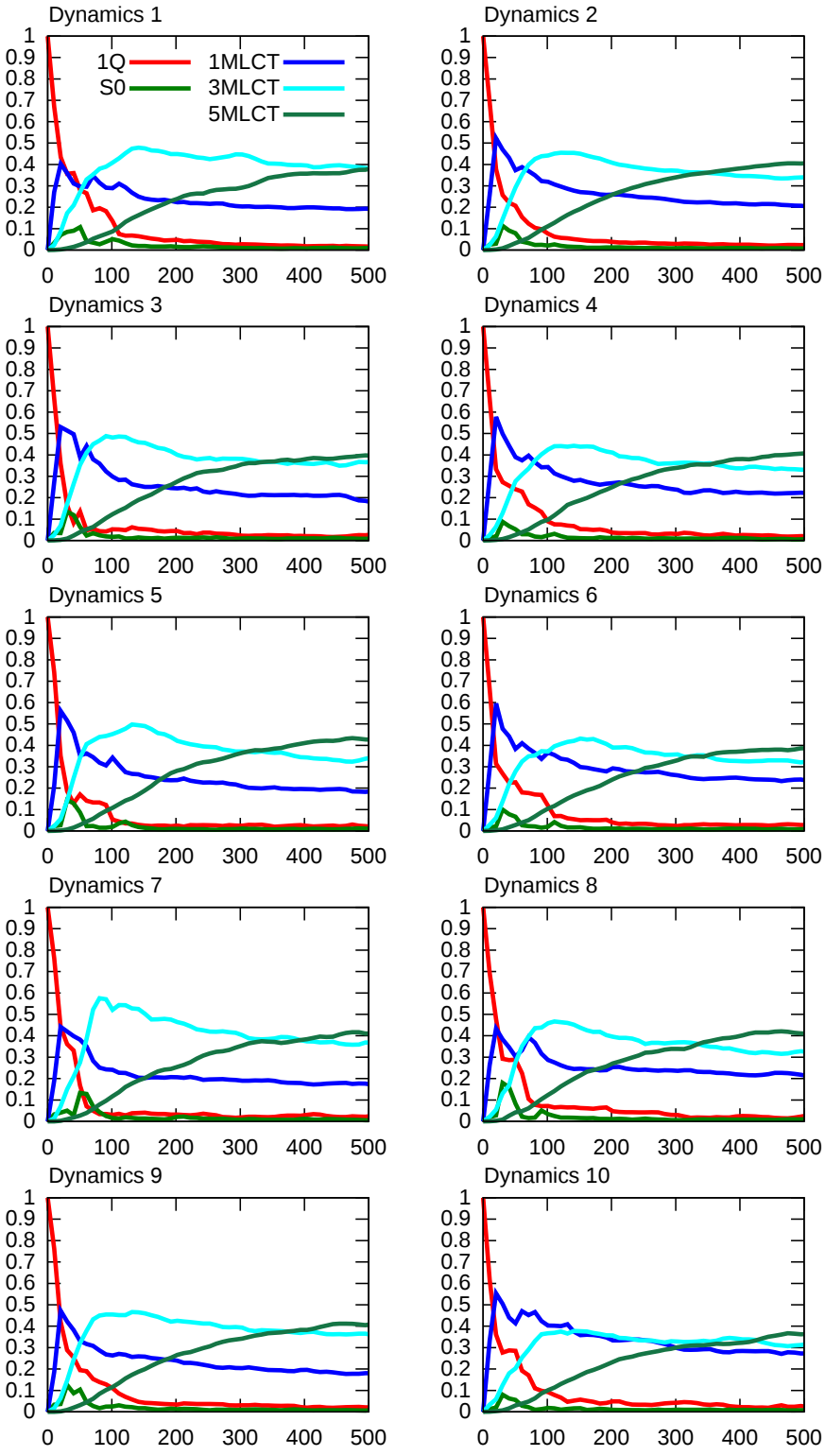

Supplementary Figure 4. Full model population evolution. Evolution of diabatic populations of the total singlet (red) triplet (green) and quintet (blue) manifold populations. Time (x-axis) is in femtoseconds.

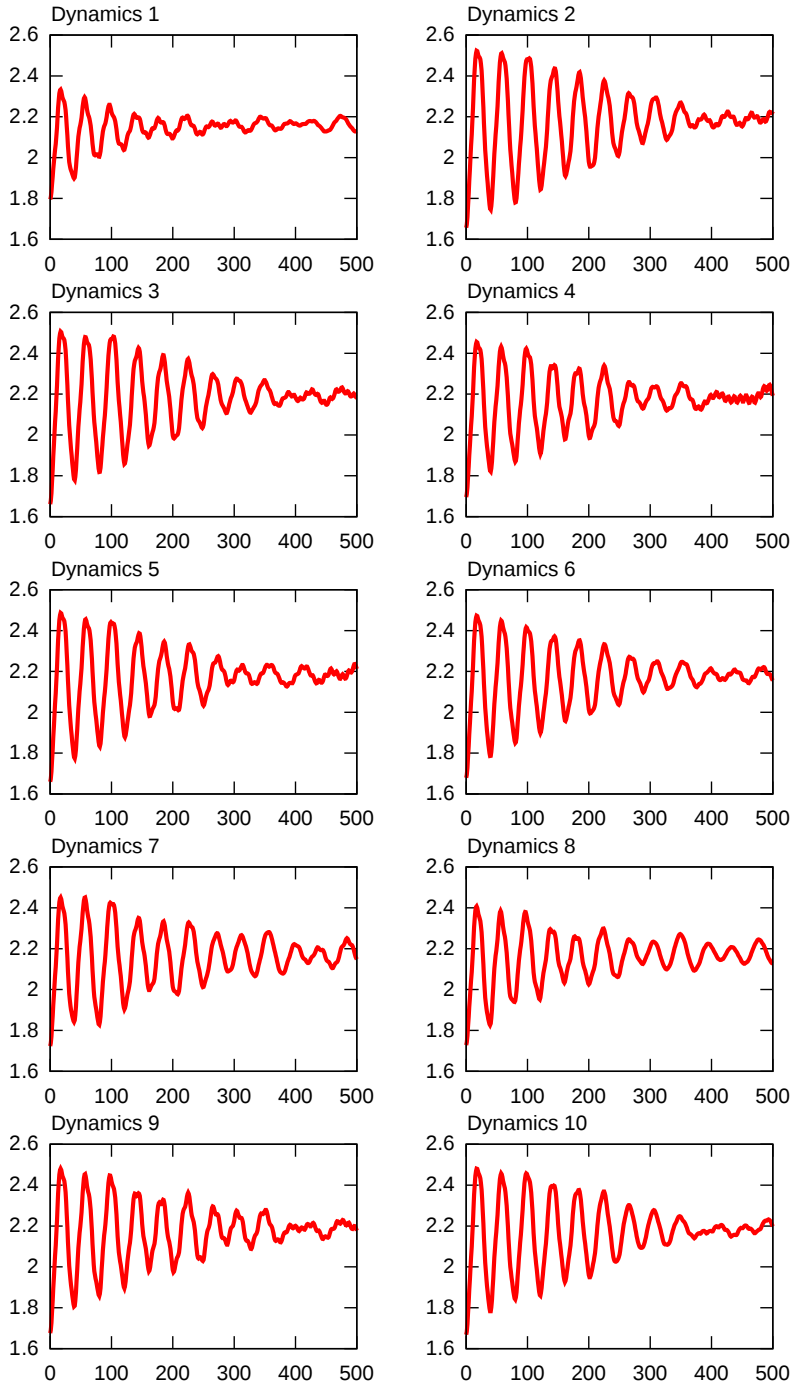

Supplementary Figure 5. Evolution of the dissociation coordinate in the full model. Evolution of the Fe-C(O) distance in Angstrom for the different initial conditions specified in Supplementary Table 8.

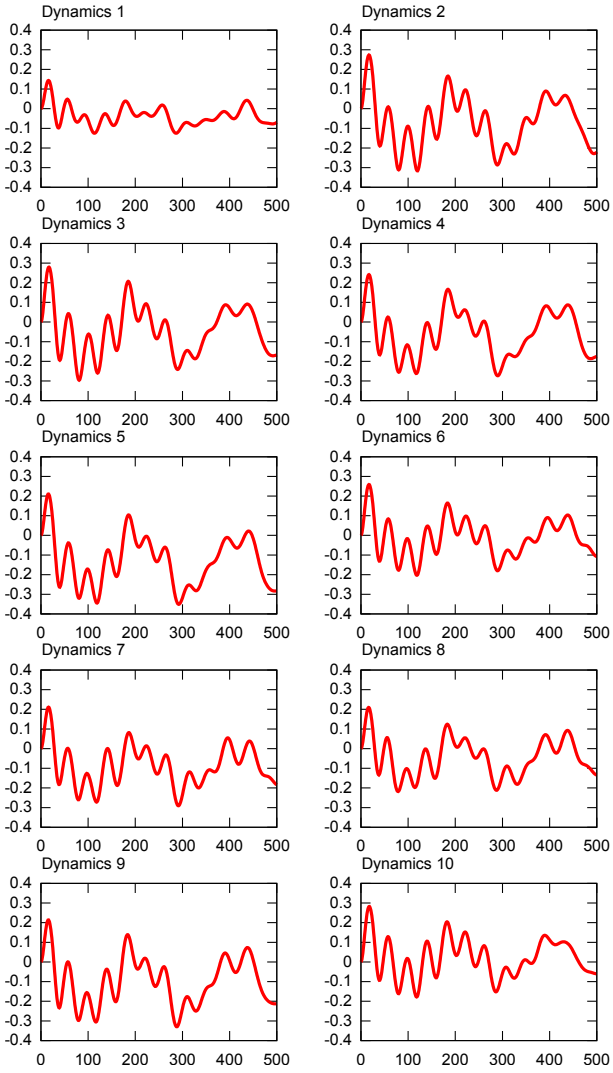

Supplementary Figure 6. Evolution of the Fe OOOP coordinate in the full model. Dynamic evolution of the Fe out-of-plane distance for the full model. The distance is calculated as the difference between the Fe z-coordinate position and the rest z-coordinate position (corresponding to the minimum energy geometry optimized at the B3LYP/LANL2DZ level). Positive and negative values of Fe indicates that Fe is going towards and contrary to the CO position respectively.

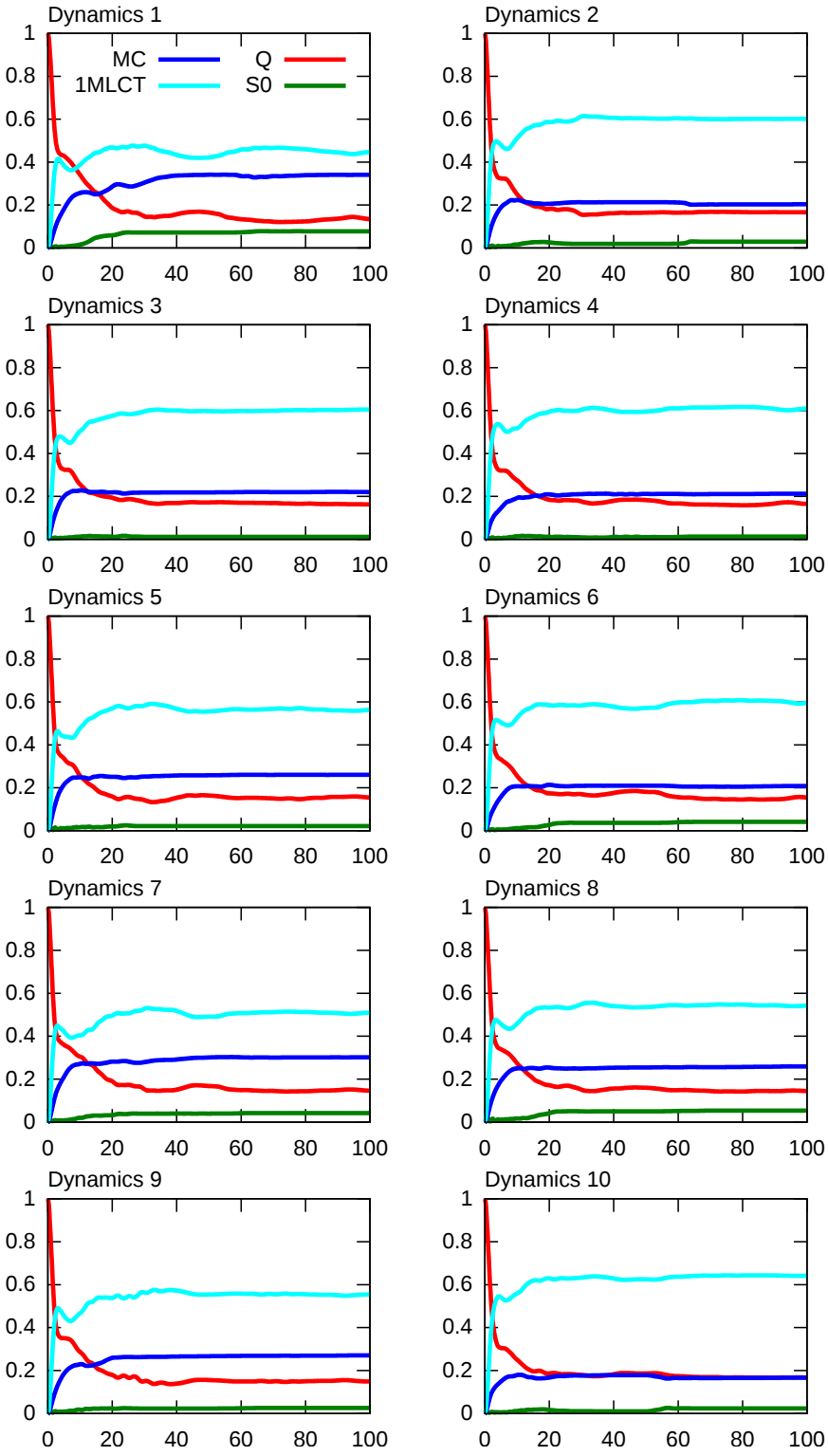

Supplementary Figure 7. Singlet manifold population evolution. Evolution of diabatic populations of the ground state S_0 (red), the summed-up populations of the metal-centred states (green), the Q-band (blue) and the MLCT band (cyan). Time (x-axis) is in femtoseconds.

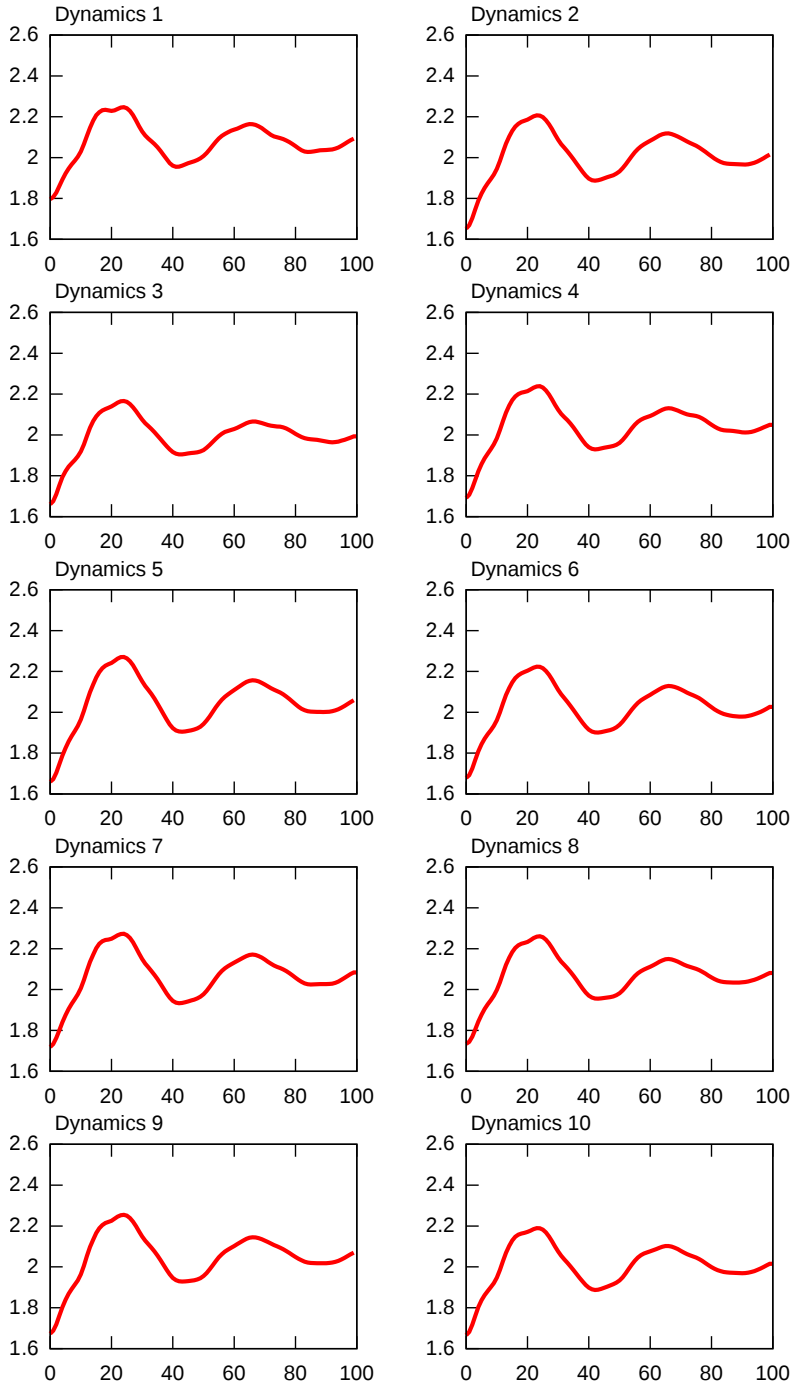

Supplementary Figure 8. Singlet manifold evolution of dissociation coordinate. Evolution of the Fe-C(O) distance (in Ångstrom) for the first 0.1 ps, using the different initial conditions specified in Supplementary Table 8.

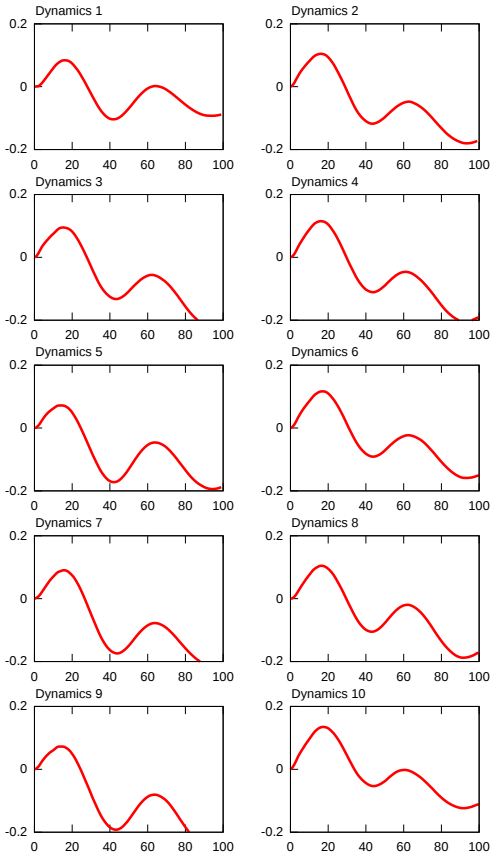

Supplementary Figure 9. Singlet manifold evolution of the Fe OOP coordinate. Dynamic evolution of the Fe out-of-plane distance for the singlet only model during the first 0.1 ps. The distance is calculated as the difference between the Fe z-coordinate position and the rest z-coordinate position (corresponding to the minimum energy geometry optimized at the B3LYP/LANL2DZ level). Positive and negative values of Fe indicates that Fe is going towards and contrary to the CO position respectively.

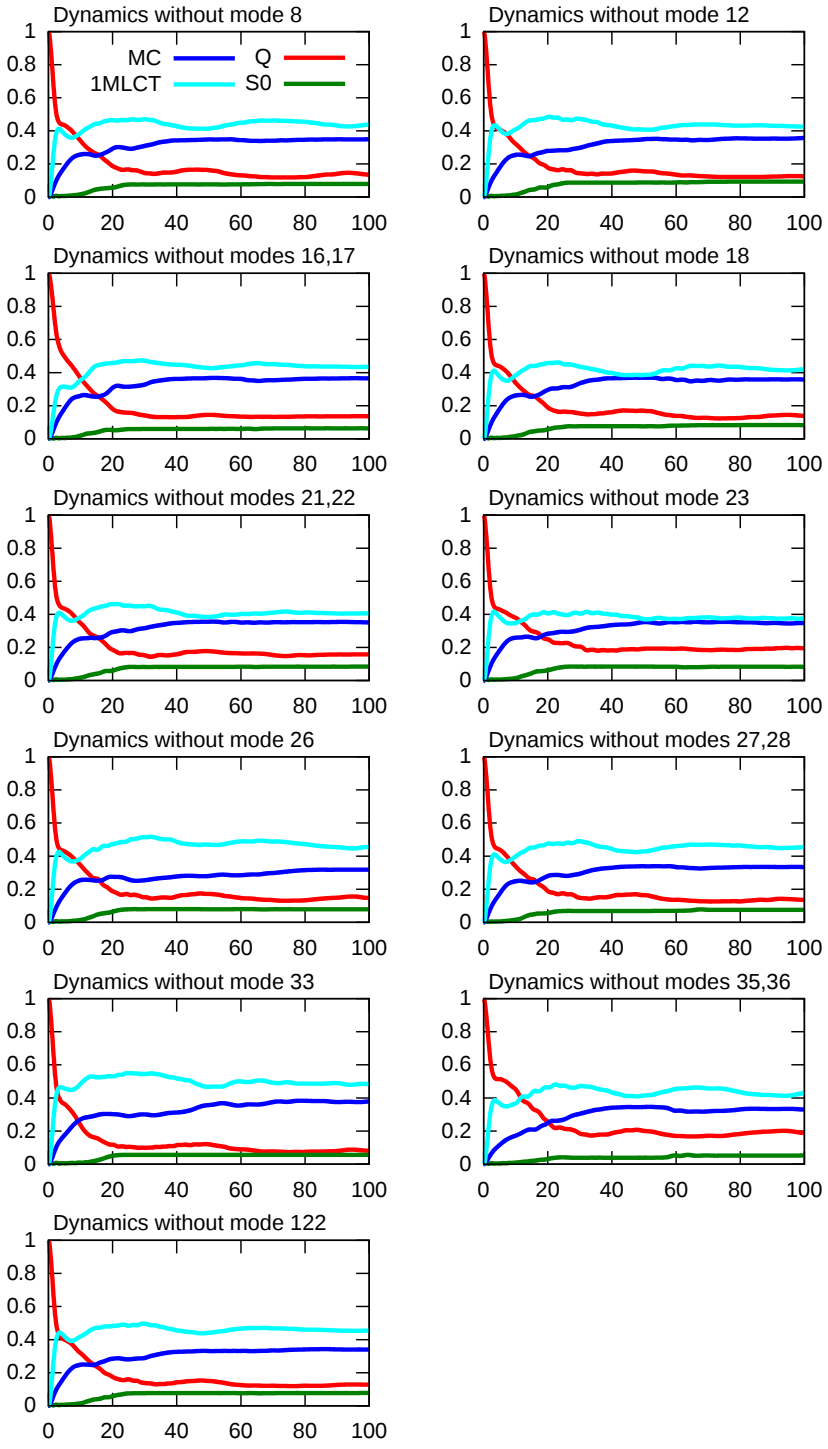

Supplementary Figure 10. Population evolution excluding normal modes. Effect of each mode on the population evolution on the singlet model. In each dynamics, we exclude the take out one mode (for singly-degenerate symmetries) or two modes (for doubly-degenerate symmetries) from the singlet model. For details of the modes, see Supplementary Table 10. The initial conditions are as in dynamics 1 of Supplementary Table 8.

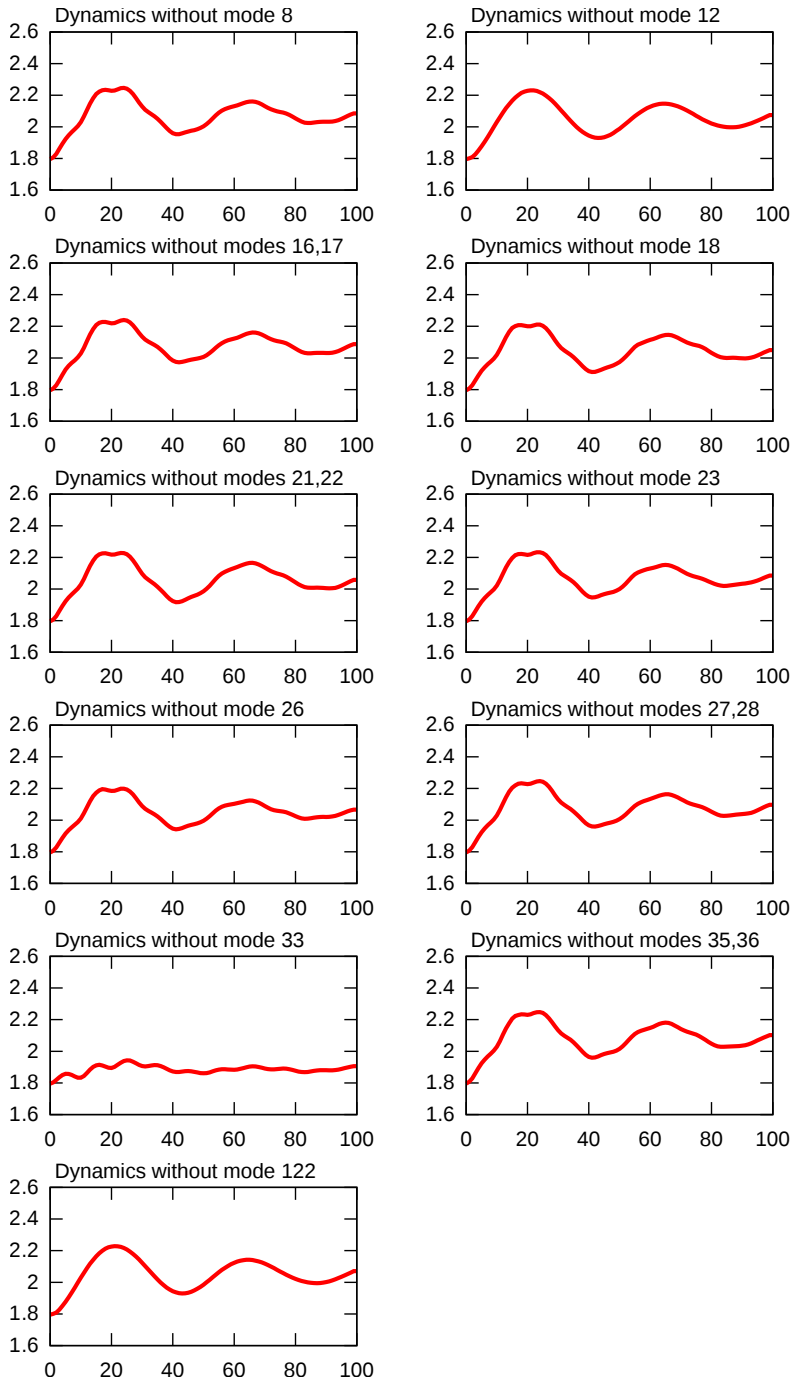

Supplementary Figure 11. Evolution of dissociation coordinate excluding certain normal modes. Evolution of the Fe-C(O) distance (in Ångstrom) for the first 0.1 ps, excluding normal modes from the dynamics (see caption of Supplementary Figure 10 for details).

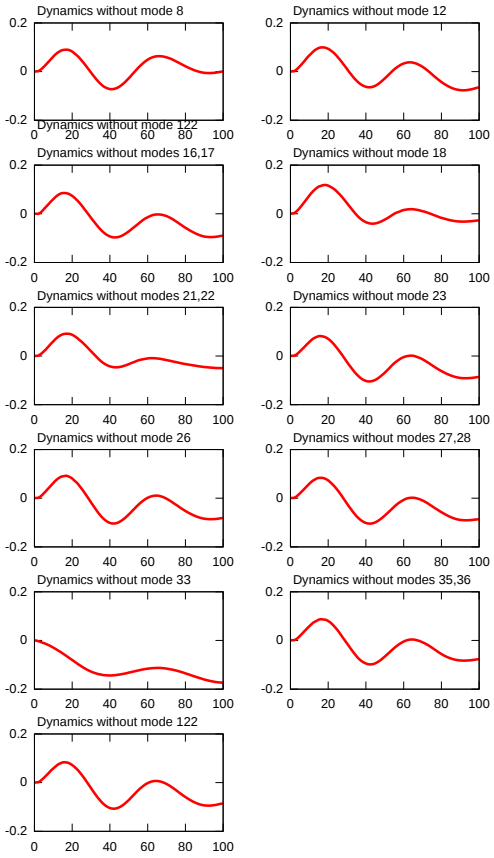

Supplementary Figure 12. Evolution of the Fe OOP coordinate excluding normal modes. Dynamic evolution of the Fe out-of-plane distance for the singlet only model during the first 0.1 ps excluding normal modes (see caption of Supplementary Figure 10 for details). The distance is calculated as the difference between the Fe z-coordinate position and the rest z-coordinate position (corresponding to the minimum energy geometry optimized at the B3LYP/LANL2DZ level). Positive and negative values of Fe indicates that Fe is going towards and contrary to the CO position respectively.

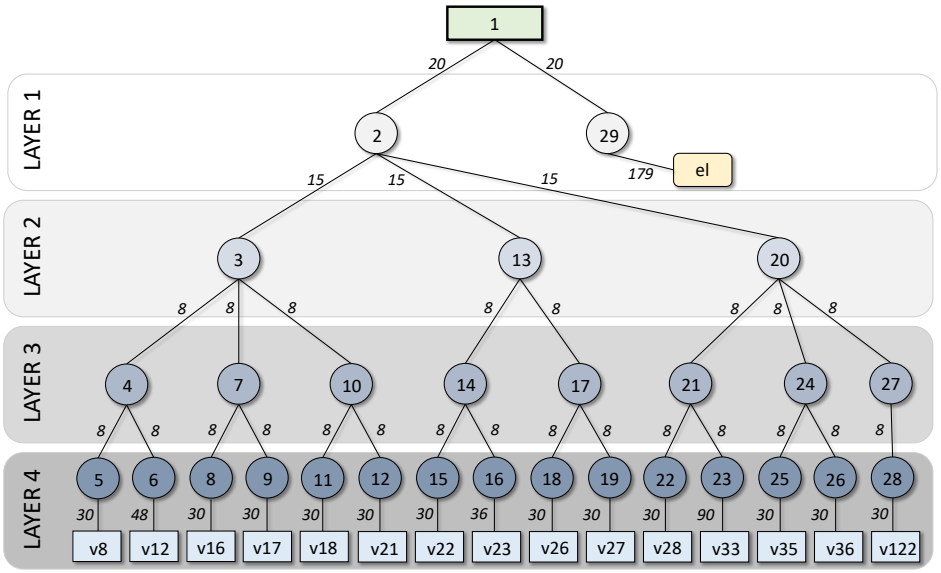

Supplementary Figure 13. Layer structure of the ML-MCTDH wavefunction. Schematic representation of the ML-MCTDH multi-layer tree structure where 179 electronic states and 15 vibrational modes are arranged into 4 layers.

Supplementary Note 1: Timescales. Due to the large number of electronic states, it is difficult to define a precise kinetic model involving each individual state. For extracting kinetic constants to be compared with experimental results, we have rather considered the following kinetic reactions:

- For the full quantum dynamics with summed up populations according to the spin multiplicity, the reaction ${}^1\mathrm{S} \xrightarrow{k_{S-T}} {}^3\mathrm{T} \xrightarrow{k_{T-Q}} {}^5\mathrm{Q}$ allows us to extract the kinetic constants corresponding to the total singlet-triplet (k_{S-T}) and the total triplet-quintet (k_{T-Q}) population transitions.
- For the full quantum dynamics with separated populations according to the state nature, the reaction ${}^1\mathrm{Q} \xrightarrow{k_Q} {}^1\mathrm{MLCT}$ allows us to extract in addition to k_Q the triplet-quintet MLCT time scale.

The fitting model for $\tau_Q = 1/k_Q$ and $\tau_{S-T} = 1/k_{S-T}$ is $\mathrm{e}^{-k_Q t}$ and $\mathrm{e}^{-k_{S-T} t}$ respectively. For $\tau_{T-Q} = 1/k_{T-Q}$ the model is 1-$\mathrm{e}^{-k_{T-Q} t}$. In Supplementary Table 9, we summarize the kinetic contants for the 10 dynamical models. The average values obtained and the standard deviation are $\tau_Q = 25.73 \pm 7.05$, τ_{S-T}=76.25 $\pm$ 15.92 and τ_{T-Q}=429.18 $\pm$ 70.06.

Supplementary Note 2: Electronic structure. All geometries have been optimized at the density functional theory (DFT) level using the LAN2DZ basis set,[2] which includes pseudopotentials to treat the relativistic effects of Fe. For such calculations, the GAUSSIAN09 software has been employed.[3] We have employed B3LYP functional for all calculations.[4–6] Tests on the B3LYP* functional (same parameters as B3LYP but employing 25% of Hartree-Fock exchange), which was reported to reproduce better the low-spin to high-spin transition was tested, but the results were not improved with respect to B3LYP.[7] It is for this reason, that the electronic structure calculations for the excited states has been performed at the CASSCF/CASPT2 level of theory.[8,9] Multi-reference calculations have been performed with Molcas 8.[10] No symmetry has been employed in the geometry optimizations, although the structures in the singlet ground state minimum show a quasi-C_{4v} symmetry. All minimum energy structures have been characterized by a frequency calculation. All CASSCF calculations have been done using 10 electrons in 9 orbitals. The orbitals are depicted in Supplementary Figure 1. In our model, we only include four orbitals for the porphyrin and five d orbitals. Since we consider the model for excitation to the Q band, we do not need to include further states for the porphyrin, and so the B band, which is located 1 ev higher than the Q band, is excluded from the system. We have selected a space of 19 singlets, 20 triplets and 20 quintets, which converge the continuum region around the Q-band. Relativistic effects have been included using the two-component Douglas-Kross-Hess Hamiltonian (DKH).[11,12] For calculating the potential energy surface, the ANO-RCC-VDZ basis set has been employed.[13,14] The effects of the basis set size are negligible (see further Supplementary Table 1). The absorption spectrum for the Imidazole-Heme-CO model, the Heme-CO model and the Imidazole-Heme can be found in Supplementary Tables 3, 4 and 5 respectively. We observe in all cases that a continuum band appears above the metal-centred states in all cases. This band is represented by configuration state functions that correspond to double (for singlet and triplet) and triple (for quintet) excitations with respect to the reference configuration. This implies that only multiconfiguration methods to the third order can be used for representing correctly the static correlation effects of the complex. Therefore, the interpretation of heme-CO complex based on the TDDFT results reported previously in the literature cannot be considered correct. The CASPT2 calculations have been performed using the multi-state approach, with an imaginary shift of 0.01 au to avoid intruder state problems. The MS-CASPT2 calculation of the potential energy surfaces has been performed freezing 50 virtual states, which accelerate the computations. Still, the spin-crossover of the ground state is qualitatively well represented. Furthermore, the minimum energy structures at the DFT level are also minima of the MS-CASPT2 protocol. The QM/MM calculations have been performed with the Tinker/Gaussian09 and Tinker/Molcas interface employing the ElectroStatic Potential Fitting method.[15] We have employed the CHARM22 force field with CMAP corrections.[16] The protein structure has been taken as the mean value X-ray structure complexed with CO of *Equus caballus* (RCSB PDB code: 5CN5).[1] The QM region comprises the full heme, the CO and the proximal histidine. A link atom has been used to cut the C_α-C_β bond. We have optimized the QM region with frozen MM region at the B3LYP/LANL2DZ level of theory. Only the water molecules appearing in the 5CN5 structure where kept and no extra water molecules were added. The electronic structure calculations have been performed with CASSCF/CASPT2/ano-rcc-vdz. Due to the computational cost, and for the sake of comparison, we have only performed the calculations over the 12 lowest roots.

Supplementary Note 3: Anharmonic couplings. In the harmonic approximation, the vibrational potential has the following form (in mass-frequency-weighted Cartesian coordinates):

$$V(q_i) = \sum_i \frac{1}{2} \omega q_i^2 \,, \tag{1}$$

Anharmonic couplings between vibrational modes can induce mode mixing, which is responsible of vibrational energy redistribution:

$$V(q_i) = \sum_i \frac{1}{2}\omega_i q_i^2 + \sum_{ijk} V_{i,j,k} q_i q_j q_k \,. \tag{2}$$

These equations are valid for the ground-state only. In the excited states, Duschinsky rotations should be included to account for the mixing of normal modes.[17] In Supplementary Table 11, we show the computed anharmonic couplings using GAUSSIAN09.[3] Remarkably, the dissociative mode (mode 33) is coupled to the doming mode (mode 26). As we have shown, the doming is activated after photolysis, and it serves to relax the structure of the high-spin state. A very strong coupling exist also between the doming mode (mode 26) with an in-plane distortion (mode 22) involving a rotation of CO. However, these modes are not directly involved in the dissociation process, and therefore it is justified to exclude them from the model. Anharmonic couplings, especially couplings to vibrational modes of the protein, will become important at times larger than 500 fs as shown experimentally.[1].

Supplementary Note 4: Quantum dynamics. Quantum dynamical calculations were carried out for the vibronic coupling Hamiltonian specified in section "Methods" of the main text, for 179 electronic states and 15 vibrational modes, using the Multi-Layer Multi-Configuration Time-Dependent Hartree (ML-MCTDH) method.[18–22] The ML-MCTDH method is a hierarchical tensor scheme which defines the wavefunction in terms of a multi-layer tree structure consisting of combinations of single-particle functions (spf's). The tree structure employed in the present calculations is illustrated in Supplementary Figure (13). Here, vertices indicate spf's (with an arbitrary numbering scheme) while edges give information on the number of spf's. Four layers were used, with the number of spf's varying between $n_{\mathrm{spf}} = 8$ and $n_{\mathrm{spf}} = 20$. All electronic states are grouped together in a formal electronic spf in the first layer. In the last layer, each one-dimensional spf is represented explicitly by a harmonic-oscillator (HO) Discrete Variable Representation (DVR) with up to 90 DVR points. The ML-MCTDH method has a unique capacity to treat the highly correlated vibronic dynamics that characterizes the present system. While full convergence is difficult to achieve, the present set of calculations are well converged in the sense that only small variations in the dynamics are observed when modifying the number of spf's.

SUPPLEMENTARY REFERENCES

[1] Barends, T. R. *et al.* Direct observation of ultrafast collective motions in CO myoglobin upon ligand dissociation. *Science* **350**, 445–450 (2015).

[2] Hay, P. J. & Wadt, W. R. Ab initio effective core potentials for molecular calculations. potentials for k to au including the outermost core orbitals. *J. Chem. Phys.* **82**, 299 (1985).

[3] Gaussian 09, Revision D.01, M. J. Frisch, G. W. Trucks, H. B. Schlegel, G. E. Scuseria, M. A. Robb, J. R. Cheeseman, G. Scalmani, V. Barone, G. A. Petersson, H. Nakatsuji, X. Li, M. Caricato, A. Marenich, J. Bloino, B. G. Janesko, R. Gomperts, B. Mennucci, H. P. Hratchian, J. V. Ortiz, A. F. Izmaylov, J. L. Sonnenberg, D. Williams-Young, F. Ding, F. Lipparini, F. Egidi, J. Goings, B. Peng, A. Petrone, T. Henderson, D. Ranasinghe, V. G. Zakrzewski, J. Gao, N. Rega, G. Zheng, W. Liang, M. Hada, M. Ehara, K. Toyota, R. Fukuda, J. Hasegawa, M. Ishida, T. Nakajima, Y. Honda, O. Kitao, H. Nakai, T. Vreven, K. Throssell, J. A. Montgomery, Jr., J. E. Peralta, F. Ogliaro, M. Bearpark, J. J. Heyd, E. Brothers, K. N. Kudin, V. N. Staroverov, T. Keith, R. Kobayashi, J. Normand, K. Raghavachari, A. Rendell, J. C. Burant, S. S. Iyengar, J. Tomasi, M. Cossi, J. M. Millam, M. Klene, C. Adamo, R. Cammi, J. W. Ochterski, R. L. Martin, K. Morokuma, O. Farkas, J. B. Foresman, and D. J. Fox, Gaussian, Inc., Wallingford CT, 2016.

[4] Becke, A. D. Density–functional exchange–energy approximation with correct asymptotic behavior. *Phys. Rev. A* **38**, 3098 (1988).

[5] Lee, C., Yang, W. & Parr, R. G. Development of the colle–salvetti correlation–energy formula into a functional of the electron density. *Phys. Rev. B* **37**, 785 (1988).

[6] Vosko, S. H., Wilk, L. & Nusair, M. Accurate spin–dependent electron liquid correlation energies for local spin density calculations: a critical analysis. *Can. J. Phys.* **58**, 1200–1211 (1980).

[7] Reiher, M., Salomon, O. & Hess, B. A. Reparameterization of hybrid functionals based on energy differences of states of different multiplicity. *Theor. Chem. Acc.* **107**, 48–55 (2001).

[8] Roos, B. J. *The Complete Active Space Self–Consistent Field Method and its Applications in Electronic Structure Calculations.*, vol. 69 of *Adv. Chem. Phys.*, 399 (John Wiley and Sons, Ltd., 1987).

[9] Andersson, K., Malmqvist, P. & Roos, B. O. Second–order perturbation theory with a complete active space self–consistent field reference function. *J. Chem. Phys.* **96**, 1218–1226 (1992).

[10] Aquilante, F. *et al.* Molcas 8: New capabilities for multiconfigurational quantum chemical calculations across the periodic table. *J. Comput. Chem.* **37**, 506–541 (2016).

[11] Douglas, M. & Kroll, N. M. Quantum electrodynamical corrections to the fine structure of helium. *An. Phys.* **82**, 89–155 (1974).

[12] Hess, B. A. Relativistic electronic-structure calculations employing a two-component no-pair formalism with external-field projection operators. *Phys. Rev. A* **33**, 3742–3748 (1986).

[13] Roos, B. O., Lindh, R., Malmqvist, P. A., Veryazov, V. & Widmark, P. O. Main group atoms and dimers studied with a new relativistic ano basis set. *J. Phys. Chem. A* **108**, 2851 (2005).

[14] Roos, B. O., Lindh, R., Malmqvist, P. A., Veryazvov, V. & Widmark, P. O. New relativistic ano basis sets for transition metal atoms. *J. Phys. Chem. A* **109**, 6575–6579 (2005).

[15] Melaccio, F., Olivucci, M., Lindh, R. & Ferré, N. Unique qm/mm potential energy surface exploration using microiterations. *Int. J. Quant. Chem.* **111**, 3339–3346 (2011).

[16] Mackerell, A. D. Empirical force fields for biological macromolecules: Overview and issues. *J. Comput. Chem.* **25**, 1584–1604 (2004).

[17] Olbrich, G. & Kupka, H. The Duschinsky effect and optical spectra. *Z. Naturforsch.* **38a**, 937–946 (1983).

[18] G. A. Worth, M. H. Beck, A. Jäckle, O. Vendrell, and H.-D. Meyer, The MCTDH Package, Version 8.5.5., see http://mctdh-uni-hd.de.

[19] Wang, H. & Thoss, M. Multilayer formulation of the multiconfiguration time–dependent hartree theory. *J. Chem. Phys.* **119**, 1289 (2003).

[20] Meyer, H.-D., Manthe, U. & Cederbaum, L. S. The multi–configurational time–dependent hartree approach. *Chem. Phys. Lett.* **165**, 73–78 (1990).

[21] Beck, M., Jäckle, A., Worth, G. & Meyer, H.-D. The multiconfiguration time-dependent Hartree (MCTDH) method: a highly efficient algorithm for propagating wavepackets. *Phys. Rep.* **324**, 1–105 (2000).

[22] Vendrell, O. & Meyer, H.-D. Multilayer multiconfiguration time-dependent Hartree method: Implementation and applications to a Henon-Heiles Hamiltonian and to pyrazine. *J. Chem. Phys.* **134**, 044135 (2011).